The Journal of Chemical Physics ARTICLE scitation.org/journal/jcp

Behavior of S, SO, and SO_3 on Pt (001), (011), and (111) surfaces: A DFT study

Cite as: J. Chem. Phys. 154, 194701 (2021); doi: 10.1063/5.0043501
Submitted: 8 January 2021 • Accepted: 26 April 2021 •
Published Online: 17 May 2021

Marietjie J. Ungerer,[1,2,a)] Cornelia G. C. E. van Sittert,[1,b)] and Nora H. de Leeuw[2,3,c)]

AFFILIATIONS

[1] Laboratory for Applied Molecular Modelling, Research Focus Area: Chemical Resource Beneficiation, North-West University, Private Bag X6001, Potchefstroom 2520, South Africa
[2] School of Chemistry, Cardiff University, Main Building, Park Place, Cardiff CF10 3AT, United Kingdom
[3] School of Chemistry, Faculty of Engineering and Physical Sciences, University of Leeds, Leeds LS2 9JT, United Kingdom

Note: This paper is part of the JCP Special Collection in Honor of Women in Chemical Physics and Physical Chemistry.
[a)] **Author to whom correspondence should be addressed:** ungerermj@cardiff.ac.uk
[b)] **E-mail:** cornie.vansittert@nwu.ac.za
[c)] **E-mail:** n.h.deleeuw@leeds.ac.uk

ABSTRACT

In the hybrid sulfur (HyS) cycle, the reaction between SO_2 and H_2O is manipulated to produce hydrogen with water and sulfuric acid as by-products. However, sulfur poisoning of the catalyst has been widely reported to occur in this cycle, which is due to strong chemisorption of sulfur on the metal surface. The catalysts may deactivate as a result of these impurities present in the reactants or incorporated in the catalyst during its preparation and operation of the HyS cycle. Here, we report a density functional theory investigation of the interaction between S, SO, and SO_3 with the Pt (001), (011), and (111) surfaces. First, we have investigated the adsorption of single gas phase molecules on the three Pt surfaces. During adsorption, the 4F hollow sites on the (001) and (011) surfaces and the *fcc* hollow site on the (111) surface were preferred. S adsorption followed the trend of $(001)_{4F} > (011)_{4F} > (111)_{fcc}$, while SO adsorption showed $(001)_{4F} > (011)_{bridge/4F} > (111)_{fcc}$ and SO_3 adsorption was most stable in a S,O,O bound configuration on the $(001)_{4F} > (011)_{4F} > (111)_{fcc}$ sites. The surface coverage was increased on all the surfaces until a monolayer was obtained. The highest surface coverage for S shows the trend $(001)_S = (111)_S > (011)_S$, and for SO it is $(001)_{SO} > (011)_{SO} > (111)_{SO}$, similar to SO_3 where we found $(001)_{SO3} > (011)_{SO3} > (111)_{SO3}$. These trends indicate that the (001) surface is more susceptible to S species poisoning. It is also evident that both the (001) and (111) surfaces were reactive toward S, leading to the formation of S_2. The high coverage of SO_3 showed the formation of SO_2 and SO_4, especially on the (011) surface. The thermodynamics indicated that an increased temperature of up to 2000 K resulted in Pt surfaces fully covered with elemental S. The SO coverage showed $\theta \geq 1.00$ on both the (001) and (011) surfaces and $\theta = 0.78$ for the (111) surface in the experimental region where the HyS cycle is operated. Lower coverages of SO_3 were observed due to the size of the molecule.

I. INTRODUCTION

The oxidation of sulfur dioxide (SO_2) in aqueous solutions has been studied for over a century.[1–3] With the advent of industrialization, automation, and massive population growth, the presence of SO_2 has increased not only as a by-product of industry but also as a result of the uses of new technologies in everyday life.[4,5] It has been shown that atmospheric SO_2 has a detrimental effect not only on the environment but also on human life.[5,6] With more countries and governments enforcing limitations on industry to reduce SO_2 emissions,[5–7] new technologies are emerging for either the capture[8] or re-utilization of SO_2.[9,10]

One viable option for the utilization of SO_2 is in the hybrid sulfur (HyS) cycle, where SO_2 reacts with water (H_2O) at temperatures between 80 and 120 °C to form sulfuric acid (H_2SO_4) and hydrogen (H_2). H_2SO_4 can be re-utilized by thermal decomposition (>800 °C) to form oxygen (O_2), H_2O, and SO_2. The net reaction of this cycle is therefore the splitting of H_2O into O_2 and H_2. In turn, H_2 is considered a potentially viable solution to address sustainable energy production as it is an ideal energy carrier, especially when coupled

with renewable sources and adequate technology,[11–14] and it is used in a variety of applications.[15–17]

Within the HyS cycle, it is well known that transition metals, even in trace amounts, are needed to catalyze the SO_2 oxidation reaction.[18–20] The current catalyst of choice is platinum (Pt), a rare and very expensive noble metal, while various other metals have been investigated,[21] i.e., Cu,[22–25] Ni,[26–28] Ag,[29,30] Rh,[31,32] and Pd[24,32–36] in addition to Pt,[24,31,37–40] which is still the best performing catalyst in terms of activity and stability.[41–43] However, major difficulties are still experienced in experiments, in part due to the occurrence of various co-adsorbed surface sulfur species, such as elemental sulfur (S), sulfur oxide (SO), and sulfur trioxide (SO_3), among others.[9]

Although sulfur is an essential element and the fifth most common element on Earth,[3,44] its presence in a catalytic environment is detrimental, causing lower yields in production and catalyst poisoning.[45] However, very little work has been performed on evaluating the energetics or thermodynamics of the adsorption of sulfur or sulfur oxides on catalyst surfaces or their surface reactions. In this paper, we have used density functional theory (DFT) calculations to predict the behavior of S, SO, and SO_3 on the Pt (001), (011), and (111) surfaces. We have examined the geometric and electronic properties of the systems, including the most stable adsorption sites, adsorption modes, and possible desorption of species that may occur, before considering increased surface coverages. Thermodynamic surface phase diagrams have also been generated by taking into consideration the surface free energies and the chemical potentials of $SO_{x,(x=0,1,3)}$.

II. COMPUTATIONAL METHODS

A. Calculation methods

Similar to the method used to study the adsorption of H_2O and SO_2,[46–48] the Vienna *Ab Initio* Simulation Package (VASP)[49–52] version 5.4.1 was used to simulate the Pt surfaces and their interaction with S, SO, and SO_3. In all calculations, the projector augmented wave (PAW)[53,54] pseudopotential was used to describe the interaction between the valence and core electrons. The core electrons were defined up to and including 5p, 3p, and 1s orbitals for the Pt, S, and O atoms, respectively. The exchange-correlation approximation was included with the Perdew–Burke–Ernzerhof (PBE)[55] functional within the generalized gradient approximation (GGA), including the D3-BJ method by Grimme with Becke–Johnson damping[56] to account for the long-range dispersion interactions[57–61] in these surface-adsorbate systems. Plane waves were included with a recommended cutoff of 400 eV. The conjugate gradient technique was adopted for all geometry optimizations and to ensure an electronic entropy of less than 1 meV $atom^{-1}$, whereas a smearing of 0.05 eV with the Methfessel–Paxton scheme of order 1[62] was used to determine the partial occupancies during geometry optimization. The final static simulations were obtained with the tetrahedron method with Blöchl corrections[63] to ensure accurate total energies, charges, and densities of states, where the electronic and ionic optimization criteria were set to 10^{-5} eV and 10^{-2} eV $Å^{-1}$, respectively.

The $Fm\bar{3}m$ crystal structure[64] of Pt was used to construct a bulk Pt structure within a primitive face-centered cubic (*fcc*) cell. The *k*-point mesh for these calculations was a Γ-centered 17 × 17 × 17 Monkhorst–Pack mesh.[65] The resulting *fcc* Pt lattice constant was 3.926 Å, which correlates with the experimental value of 3.925 Å.[66,67] The low Miller index Pt (001), (011), and (111) surfaces were created with the METADISE code.[68] Periodic p(3 × 3), p(3 × 3), and p(4 × 4) supercells were constructed, respectively, each with four layers and a 15 Å vacuum space to ensure that no interaction would occur between the adsorbates and surfaces in neighboring simulation cells deriving from the three-dimensional boundary conditions. All three surfaces are bulk terminated 2 × 2 structures with four atomic layers, with the surface simulation cells containing 72, 72, and 64 atoms, respectively. The Brillouin zone was sampled by a Γ-centered 7 × 7 × 1 Monkhorst–Pack *k*-point grid. During the optimization of the surfaces, the bottom two layers of the supercells were frozen in their bulk locations, with the remaining two layers allowed to move until the set energy criteria were met. Even though Pt does not have unpaired electrons, spin polarization was considered during these surface calculations, as future work will also include base metal dopants such as Ni and Co, for which this would be necessary.

For the calculations of the geometrical properties, adsorption, and electronic properties, the isolated S, SO, and SO_3 molecules were modeled in a periodic box of 12 × 13 × 14 $Å^3$ to ensure negligible interaction with neighboring cells. For both the geometry optimizations and energy calculations, the Gaussian smearing[62] of 0.05 eV was used with a Γ-centered Monkhorst–Pack[65] *k*-point mesh of 1 × 1 × 1. None of the adsorbate molecules were computed with symmetry constraints, but for increased accuracy, dipole corrections were added in all directions. Spin polarization was considered both for the isolated molecules and in the adsorption calculations. The breakdown of charge transfer between the adsorbates and the surfaces was obtained via the Bader analysis,[69–72] assigning the electron density of molecules and solids to individual atoms or regions enclosed by local minima in the charge density.

B. Coverage-dependent surface energies

The standard calculation[58,73] of the surface energies for relaxed and unrelaxed systems was used. To calculate the average adsorption energy (E_{ads}) per adsorbate molecule (S, SO, and SO_3) adsorbed onto the Pt surface, the following equation was used:[46–48,74]

$$E_{ads} = \frac{1}{N_{SO_x}}\left[E_{Pt,r}^{N_{SO_x}\neq 0} - \left(E_{Pt,r}^{N_{SO_x}=0} + N_{SO_x}E_{SO_x}\right)\right], \quad x = 0, 1, 3, \tag{1}$$

where N_{SO_x} is the number of adsorbed S, SO, or SO_3 molecules, $E_{Pt}^{N_{SOx}\neq 0}$ is the energy of the Pt slab with adsorbed SO_x molecules, $E_{Pt}^{N_{SOx}=0}$ is the energy of the clean Pt surface, and E_{SO_x} is the energy of the isolated $SO_{x,(x=0,1,3)}$ molecule after relaxation. Another measure of adsorption is the energy of sequential adsorption (Sequential E_{ads}),[47] indicating the difference in energy as coverage increases,

$$Seq \cdot E_{ads} = \left[E_{Pt,r}^{N_{SO_x}\neq 0_{(i+1)}} - \left(E_{Pt,r}^{N_{SO_x}\neq 0_i} + E_{SO_x}\right)\right], \quad x = 0, 1, 3, i = 0, 1, \ldots, N, \tag{2}$$

thereby calculating the energy difference between that of an adsorbate system with one more adsorbate $E_{Pt}^{N_{SOx}\neq 0_{(i+1)}}$ and the previous system with one less adsorbate ($E_{Pt}^{N_{SOx}\neq 0_{(i)}}$).

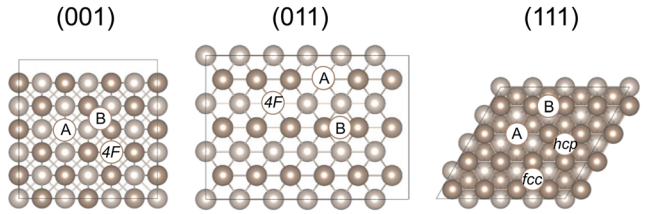

FIG. 1. Top views of the Pt (001), (011), and (111) surfaces with the adsorption sites indicated as four-fold hollow (4F), bridge (B), atop (A), face-cubic centered (*fcc*), and hexagonal close packed (*hcp*). All Pt atoms are gold in color throughout the paper, while the second layer is displayed in a lighter color to distinguish between top layer and subsequent layer atoms.

The surface coverage (θ) is defined as the number of adsorbed SO_x molecules (N_{SO_x}) divided by the number of adsorption sites (N), as denoted by

$$\theta = \frac{N_{SOx}}{N}. \tag{3}$$

If no adsorption has taken place, $\theta = 0$, whereas for full coverage, i.e., when a monolayer has formed on the surface, $\theta = 1$. The most stable configurations of the (001), (011), and (111) surfaces were used to investigate surface coverage, with the surface simulation cells having 9, 18, and 9 adsorption sites (N), respectively. To incorporate the thermodynamic effect of the different coverages of $SO_{x,(x=0,1,3)}$ on the Pt (001), (011), and (111) surfaces, the correlating surface free energies (σ) are compared at different temperatures (T) and the $SO_{x,(0,1,3)}$ chemical potential (μ_{SOx}). To this end, we have followed an established method[74] to determine the thermodynamic effect of the adsorption of SO_2[47,48] and H_2O[46] on these Pt surfaces. The resulting change in surface free energy resulting from the SO_x adsorption was calculated as follows:

$$\Delta\sigma(T,p) = \frac{1}{A_{surface}}[E_{Pt,r}^{N_{SO_x}\neq 0} - E_{Pt,r}^{N_{SO_x}=0} - N_{SO_x}\cdot\mu_{SO_x}]. \tag{4}$$

In order to calculate the surface free energy as a function of temperature and pressure, we also require the chemical potential of the SO_x species $\mu_{SO_x}(T,p_0)$, which we have obtained from experimental values,[46–48] by extracting the chemical potential from ideal gas values in thermodynamic tables.[75] The chemical potential of the $SO_{x,(x=0,1,3)}$ species in the gas phase has been reported before[76] and can be expressed as

$$\mu_{SO_x}(T,p) = E_{SO_x}^{ZPE} + \Delta G_{SO_x}(T,p_0) + k_B T \ln\frac{p}{p_0}, \tag{5}$$

where the zero-point energy $E_{SO_x}^{ZPE}$ includes the contributions from rotation and vibrations of the SO_x molecule, and the Gibbs free energy difference $\Delta G_{SOx}(T,p_0)$ is per SO_x molecule for temperatures between 0 K and T at p_0 = 1 bar. The final term ($k_B T \ln\frac{p}{p_0}$) denotes the free energy change of SO_x gas at constant temperature (T) when the partial pressure changes from p_0 to p.

III. RESULTS AND DISCUSSION

A. Pt (001), (011), and (111) surfaces

Figure 1 shows the three Pt surfaces under consideration with possible adsorption sites for each surface. The *fcc* arrangement of Pt resulted in the flat smooth Pt (001) and Pt (111) structures and a corrugated or grooved Pt (011) surface. The surface energy of each surface correlates with experimental[77] and modeled values[78] and followed the observed trend Pt (111) < Pt (001) < Pt (011) at 2.046, 2.462, and 2.615 J/m^2, respectively. Both Pt (001) and Pt (011) have three adsorption sites, indicated by atop (A), bridge (B), and four-fold hollow (4F), while Pt (111) has four sites indicated by atop (A), bridge (B), face-cubic centered (*fcc*), and hexagonal close packed (*hcp*). All the Pt atoms throughout this paper are gold colored, but for clarity the second layer atoms below the top surface are displayed in a lighter color.

B. S adsorption and surface coverage

Only one atom of elemental sulfur (S) was considered for adsorption in all adsorption sites on all three Pt surfaces. The most stable adsorptions are shown in Fig. 2 with the adsorption energies (E_{ads}), charge transfer, and bond distance (d) of the adsorbed S on the Pt (001), (011), and (111) surfaces listed in Table I. The most stable adsorption with regard to adsorption energy was on the Pt (001) surface at −7.09 eV followed by both Pt (011) and Pt (111) with adsorption energies ranging between −5.1 and −5.5 eV. Alfonso[79] also showed that the most stable S adsorption on Pt (111) occurs in

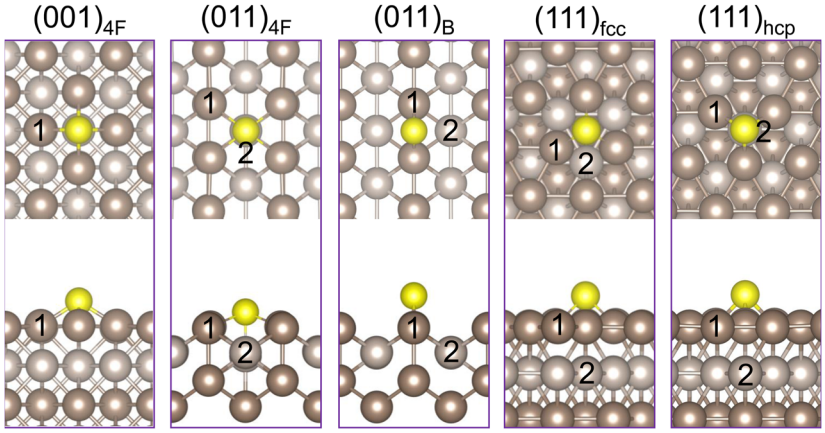

FIG. 2. Stable absorption sites of S on Pt (001), (011), and (111) surfaces. The atom color yellow denotes sulfur atoms. The numbers (1, 2) in indicate the significant Pt atoms in the surface (1) or in the second layer (2).

TABLE I. Adsorption energies (E_{ads}), charge transfer, and bond distance (d) of the adsorbed S on the Pt (001), (011), and (111) surfaces with $\theta_{(001)/(111)} = 0.11$ and $\theta_{(011)} = 0.06$. The numbers (Pt_1, Pt_2) indicate the significant Pt atoms in the surface or in the second layer, as shown in Fig. 2.

		$(001)_{4F}$	$(011)_{4F}$	$(011)_B$	$(111)_{fcc}$	$(111)_{hcp}$
	E_{ads} (eV)	−7.09	−5.47	−5.14	−5.47	−5.26
	Δq (e)	−0.07	−0.25	−0.08	−0.06	−0.18
d (Å)	S–Pt_1	2.35	2.46	2.20	2.26	2.26
	S–Pt_2	⋯	2.34	3.61	4.14	3.87

the *fcc* site (−5.23 eV) followed by the *hcp* site (−5.03 eV). In both Pt (001) and Pt (011) surfaces, the S atom prefers the 4F hollow adsorption site, whereas on the (111) surface, both *fcc* and *hcp* hollow sites are preferred. Rodríguez and Santana[80] have shown that S adsorption is most stable on the $(100)_{4F}$ surface (−5.16 eV) followed by the $(111)_{fcc}$ surface (−4.63 eV) and then the (110) surface (−4.37 eV), however, in the B site rather than the 4F binding site. From the charge analysis in Table I, the negative values of Δq indicate the charge transfer from the surface to the adsorbate, where most of the charges were transferred to the $(011)_{4F}$ site, followed by $(111)_{hcp}$, $(011)_B$, $(011)_{4F}$, and $(111)_{fcc}$. Interestingly, in the of the $(001)_{4F}$, $(011)_B$ and $(111)_{fcc}$ sites, S is surrounded by various Pt atoms in the surface, but none in the second layer just below the S atom, whereas in the $(011)_{4F}$ and $(111)_{hcp}$ sites, a Pt atom in the second layer is located below the S atom, contributing to the higher electron transfer observed (Table I). The adsorption energy for $N_S = 1$ was calculated to be most favorable on the (001) surface followed by the (011) and (111) surfaces, which is the same trend as was found for H_2O and SO_2 adsorption.[46–48]

The most stable configurations [$(001)_{4F}$, $(011)_{4F}$, and $(111)_{fcc}$] were used to investigate surface coverage by increasing the number of adsorbed S atoms ($N_{SO_x}, x = 0$) on each Pt surface until a monolayer (ML) was obtained. To obtain the lowest energy configurations, shown in Fig. 3, various placements of subsequent S atoms were considered. To determine if adsorption is still favored as the surface coverage increases, the average adsorption energy as a function of surface coverage is shown in Fig. 4(a), whereas the sequential adsorption energy as a function of surface coverage is shown in Fig. 4(b).

Not surprisingly, more S atoms could be adsorbed onto the Pt surfaces than H_2O[46] or SO_2[47] molecules. On the (001) surface, as the surface coverage increases up to $\theta = 1.11$, the mode of adsorption remained the same; no recombination occurs during the geometry optimizations. However, as the coverage increased to $\theta = 1.22$, the surface became "crowded" and the S atoms are no longer perfectly adsorbed in the 4F hollow. At $\theta = 1.34$, the S atoms surrounded one of the surface Pt atoms and displaced it out of the surface plane and two S_2 molecules formed on the surface. This behavior confirms experimental reports[9] that Pt electrodes are poisoned and, in extreme cases, delamination of Pt occurs when S deposition is detected on the surface. The average adsorption energy is calculated as a function of the surface coverage of S, i.e., the total adsorption energy divided by the maximum number of binding sites, i.e., 9, 18, and 9 for the (001), (011), and (111) surface, respectively. Figure 4(a) shows that the same trend is observed as in previous studies on H_2O and SO_2 adsorption, where E_{ads} decreases with increased θ. The sequential adsorption also shows that up to $\theta = 1.11$, E_{ads} decreases. However, at higher coverages $\theta \geq 1.22$, E_{ads} increases due to the formation of S_2. In addition, as Pt is displaced into the vacuum, the surface becomes more unstable and less active, which can also cause E_{ads} to increase.

On the (011) surface, when adsorption was increased to $\theta = 1$, no S recombination or Pt delamination occurred. At $\theta > 1$, a second layer of S started to form, showing that the (011) surface was less reactive. Similar to the (001) surface, the average E_{ads} decreases with increasing θ, but the sequential E_{ads} did not show a clear trend.

The Pt (111) surface showed no reactivity or delamination up to $\theta = 0.89$. However, when all nine *fcc* sites were filled ($\theta = 1$), S started to adsorb onto the *hcp* sites, resulting in the formation of S_2. More pairs of S_2 formed as the S adsorption continued up to $\theta = 1.33$. Higher coverage was not obtained, however, as a second layer started forming. Due to the formation of S_2, not all the S atoms were adsorbed onto the *fcc* sites and no Pt displacement was observed. Similar to the other two surfaces, E_{ads} increased as θ increased, which was also observed in the sequential E_{ads} data. With the formation of the S_2 molecules, E_{ads} increased slightly.

Comparing the increase in coverage on all three Pt surfaces, it was seen that the highest coverage of S was obtained on the (001) and (111) surfaces followed by the (011) surface. In addition, both the (001) and (111) surfaces were reactive toward the formation of S_2 and Pt degradation.

C. SO adsorption and surface coverage

Three modes of SO adsorption on the metallic surfaces have been investigated, including S-bound, O-bound, and S,O-bound on all the adsorption sites shown in Fig. 1. The most stable structures for the SO adsorption on the Pt surface in terms of adsorption energy are shown in Fig. 5. The correlating adsorption energy, bond distances, and angles, and charge transfer of the adsorbed SO, with respect to the Pt surfaces, are shown in Table II.

Three stable SO adsorption configurations were obtained for the (001) surface. All three were on the 4F binding site, with the highest adsorption energy achieved where S was bound to the Pt surface and the O directed away, i.e., $4F_{S\text{-bound}}$, followed by two configurations where both S and O were bound to Pt. In the first configuration, $4F_{S,O\_A}$, the S atom is bound to two Pt atoms on opposite sides of the 4F hollow, with the O atom bound to a third Pt atom; in the second configuration, $4F_{S,O\_B}$, both the S and O atoms are bound to two Pt atoms on either side of the 4F hollow, as shown in Fig. 5. We note that the charge transfer is lowest (−0.07 e^-) when only one S is bound to the Pt surface followed by the tri-bound $4F_{S,O\_A}$ (−0.21 e^-) and the tetra-bound $4F_{S,O\_A}$ (−0.41 e^-) configurations. When comparing the S–O bond length, it can be seen that the adsorption configuration can cause a deviation of up to 0.2 Å from the experimentally measured S–O bond length of 1.44 Å,[81] which correlates with the $4F_{S\text{-bound}}$ structure. This shows that the bond lengths and charge transfer are dependent on the bond order and type of bond formed during adsorption.[82]

On the Pt (011) surface, four stable adsorption configurations were observed: one being S-bound and three S,O-bound. Energetically, the most stable is the tetra-bound configuration $4F_{S,O}$, within a 4F hollow, following the groove on the (011) surface, closely followed by the tri-bound $Bridge_{S,O}$ where SO is again in the 4F hollow,

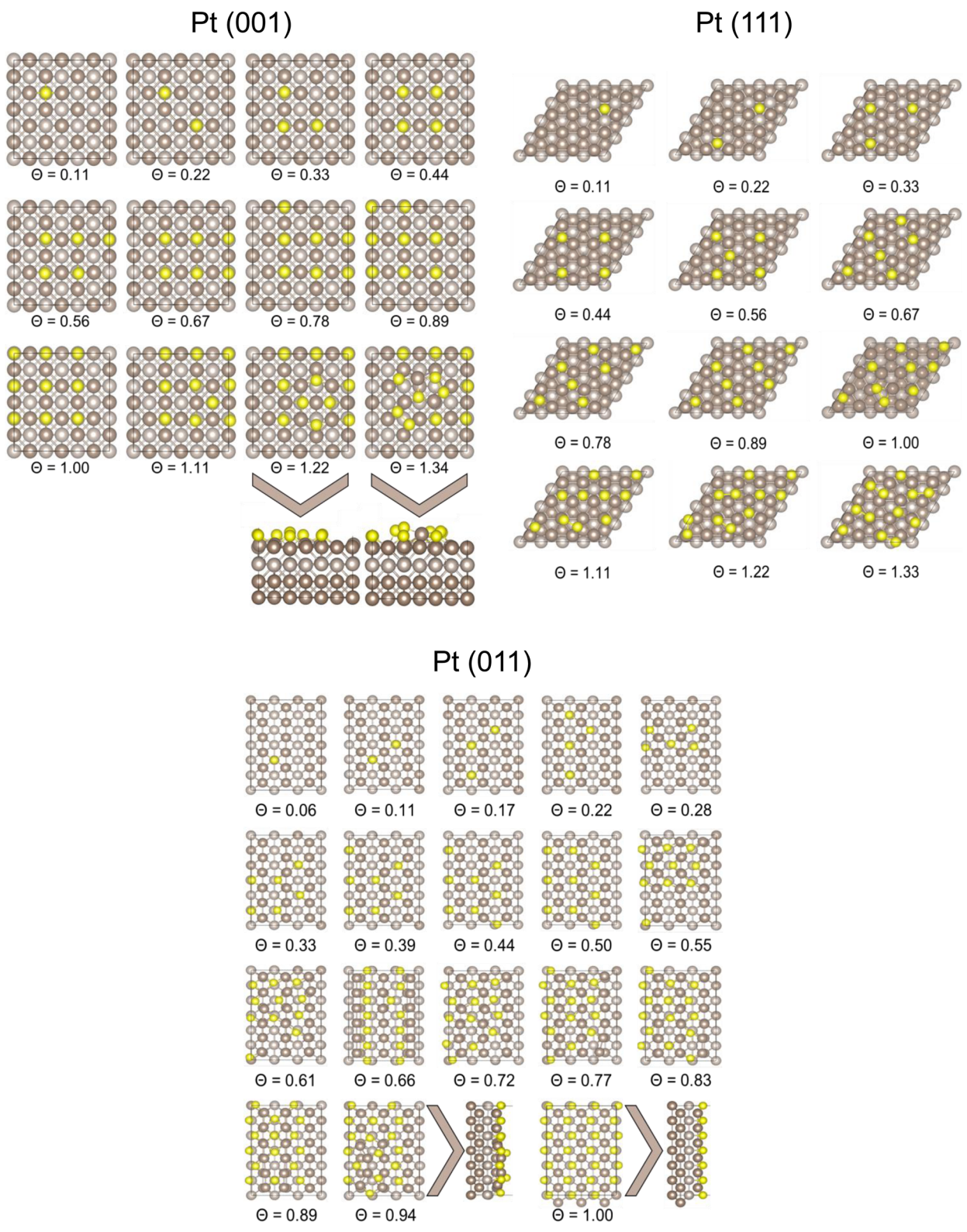

FIG. 3. Increased adsorption coverage of S on Pt (001), (011), and (111) surfaces.

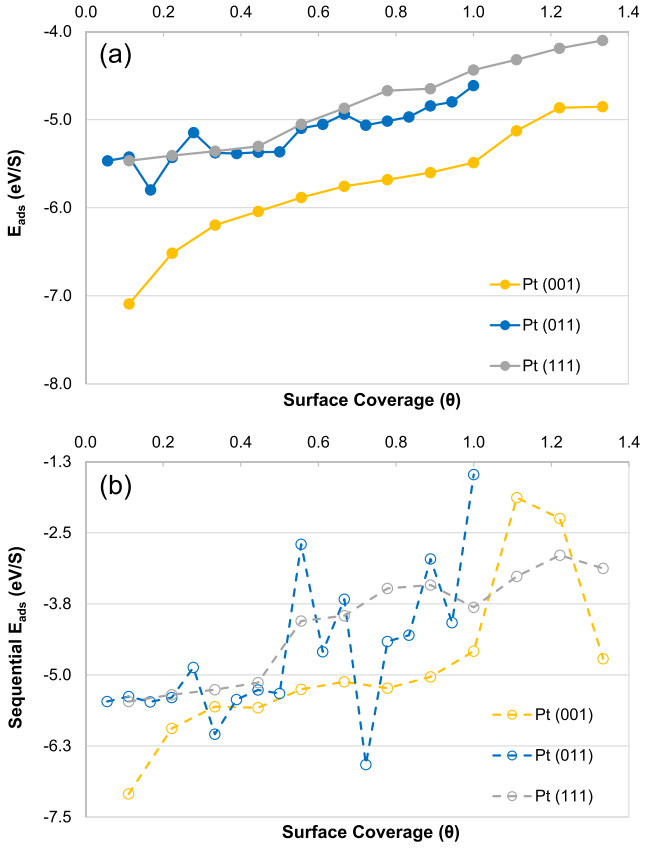

FIG. 4. Average (a) and sequential (b) adsorption energies (E_{ads}) as a function of S surface coverage (θ) on the Pt (001), (011), and (111) surfaces.

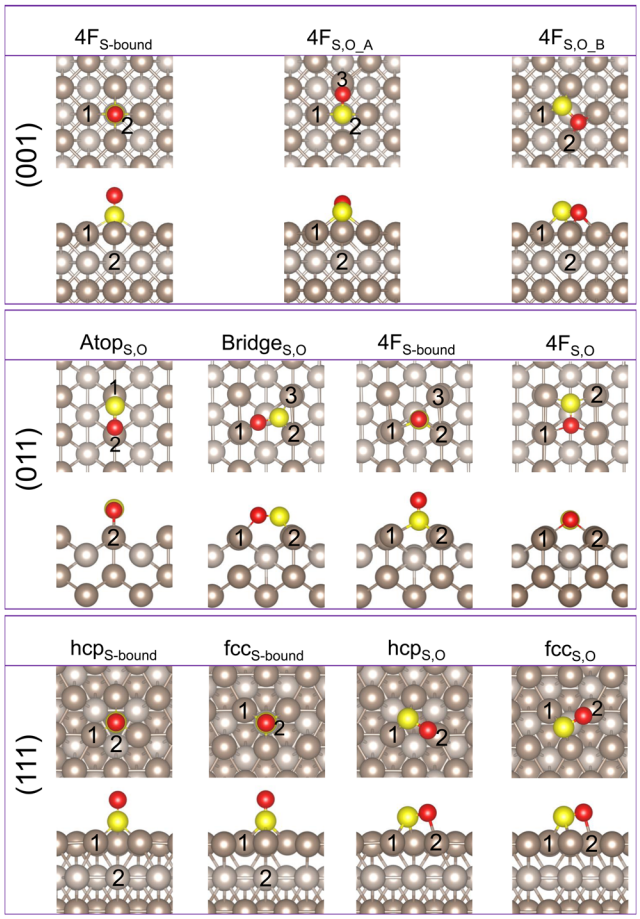

FIG. 5. Stable absorption sites of SO on Pt (001), (011), and (111) surfaces. The atom colors yellow and red denote sulfur and oxygen atoms, respectively. The numbers (1, 2) indicate the significant Pt atoms in the surface (1) or in the second layer (2).

but across the (011) groove. The third most stable configuration is $4F_{S\text{-bound}}$, with a bidentate S offset from the 4F hollow, followed by the fourth configuration, $Atop_{S,O}$ where S,O forms a bidentate configuration on the ridge of the (011) surface between two Pt atoms, as shown in Fig. 5. Similar to the (001) surface, the charge transfer is dependent on the bond orders $4F_{S,O}$ (4) > $Bridge_{S,O}$ (3) > $4F_{S\_bound}$ (2) > $Atop_{S,O}$ (2). As on the (001) surface, the S–O bond length of $4F_{S\text{-bound}}$ correlates with the free S–O bond length but in the other cases deviates by up to 0.15 Å,[81] depending on the adsorption configuration.

The (111) surface achieved four stable adsorption configurations, with either a S,O-bonded or a S-bound geometry on both the *fcc* and *hcp* binding sites, i.e., $fcc_{S,O}$, $fcc_{S\text{-bound}}$, $hcp_{S,O}$, and $hcp_{S\text{-bound}}$, respectively. Similar to the (001) surface, the adsorption energy was the highest for the S-bound configurations, $hcp_{S\text{-bound}}$ > $fcc_{S\text{-bound}}$ followed by the S,O-bound configurations, $hcp_{S,O}$ > $fcc_{S,O}$. Similar to the trends observed on both the (001) and (011) surfaces, the charge transfer increased as the bond order increased, $fcc_{S\text{-bound}}$. < $hcp_{S\text{-bound}}$ < $fcc_{S,O}$ < $hcp_{S,O}$. As on the (011) surface, the S–O bond length of S-bound configurations ($fcc_{S\text{-bound}}$. and $hcp_{S\text{-bound}}$) correlates with the free S–O bond length, but it is elongated by 0.1 Å in the S,O-bound configurations ($fcc_{S,O}$ and $hcp_{S,O}$).

Similar to the adsorption of S, H_2O, and SO_2, the adsorption energy for N_{SO} = 1 was calculated to be most favorable on the (001) surface followed by the (011) and (111) surfaces.[46–48] The most stable SO configurations on all three Pt surfaces were used to investigate the effect of surface coverage. However, on the (011) surface, the $4F_{S,O}$ and $Bridge_{S,O}$ had similar adsorption energies, and thus, the four configurations considered included $(001)_{4F\_S}$, $(011)_{4F\_S,O}$, $(011)_{B\_S,O}$, and $(111)_{hcp\_S}$, as shown in Fig. 6.

As with the adsorption of S, the number of adsorbed SO molecules (N_{SO_x}, x = 1) is increased on each Pt surface until a monolayer was obtained. Figure 7 shows the corresponding surface coverage as a function of both adsorption energy (a) and sequential adsorption energy (b). As with the adsorption of elemental S, it can be seen that on the Pt (001), E_{ads} decreases steadily as the surface coverage is increased, in correlation with the sequential E_{ads} up to θ = 1. At this stage, all the 4F hollow adsorption sites are occupied and very stable. However, at θ = 1.11, one of the SO molecules is bound atop a Pt atom, which is pulled out from the surface, causing the sequential E_{ads} to decrease. When a second SO molecule was

TABLE II. Adsorption energies (E_{ads}), bond distances, (d), and angles (∠) of the adsorbed SO on the Pt (001), (011), and (111) surfaces, with the relevant charge transfers (Δq) following adsorption, with $\theta_{(001)(111)} = 0.11$ and $\theta_{(011)} = 0.06$. The numbers (Pt_1, Pt_2) indicate the significant Pt atoms in the surface or in the second layer shown in Fig. 5.

		(001)			(011)				(111)			
		$4F_S$	$4F_{S,O\_A}$	$4F_{S,O\_B}$	$Atop_{S,O}$	$Bridge_{S,O}$	$4F_S$	$4F_{S,O}$	hcp_{S}	fcc_{S}	$hcp\_{S,O}$	$fcc\_{S,O}$
	E_{ads} (eV)	−5.10	−4.83	−4.12	−3.01	−3.56	−3.17	−3.57	−3.39	−3.25	−3.19	−3.10
	Δq (e)	−0.07	−0.21	−0.41	−0.17	−0.21	−0.07	−0.26	−0.17	−0.12	−0.25	−0.23
d (Å)	S–Pt_1	2.33	2.32	2.23	2.15	3.35, 2.30 (Pt_3)	2.38, 2.43 (Pt_3)	3.19	2.23	2.23	2.26	2.26
	S–Pt_2	3.35	3.58	3.10	2.97	2.21	2.25	2.26	4.10	3.84	2.85	2.85
	O–Pt	3.35 (Pt_1)	2.10 (Pt_3)	2.19 (Pt_2)	2.06 (Pt_2)	2.15 (Pt_1)	2.31 (Pt_1)	2.40 (Pt_1)	3.35 (Pt_1)	3.37 (Pt_1)	2.15 (Pt_2)	2.18 (Pt_2)
	S–O	1.47	1.60	1.67	1.58	1.57	1.48	1.63	1.46	1.46	1.56	1.56
∠ (°)	O–S–Pt	121.8 (Pt_1)	103.12 (Pt_1)	103.6 (Pt_1)	106.1 (Pt_1)	112.1 (Pt_2)	115.9 (Pt_1)	104.3 (Pt_2)	129.2 (Pt_1)	130.8 (Pt_1)	106.8 (Pt_1)	105.2 (Pt_1)
	SO-surf⊥	89.7	21.02	79.6	16.1	14.9	2.7	91.6	92.6	93.4	30.4	32.2

added in the atop site, again a Pt atom was displaced from the surface, indicating that it is not only elemental S, which causes Pt delamination in a catalytic environment, but that the presence of SO can also cause surface destabilization and possibly catalyst degradation. At $\theta > 1.22$, a second layer of SO started to form, but there was no evidence that SO molecules reacted with each other.

As on the (001) surface, on the Pt (011) surface E_{ads}, decreased linearly as θ increased for both $4F_{S,O}$ and $Bridge_{S,O}$ adsorption configurations until full coverage ($\theta = 1$) was obtained. Comparing the sequential E_{ads} for both of these adsorptions, it can be seen that in the $4F_{S,O}$ case, E_{ads} plateaus up to a coverage of $\theta = 0.55$. At coverages $0.55 < \theta < 0.73$, the surface becomes crowded, causing the sequential E_{ads} to decrease significantly, due to a change in SO adsorption. However, at $\theta = 0.77$, the sequential E_{ads} increased sharply due to all the SO molecules aligning in a similar fashion to the single SO adsorption configuration. At $\theta = 1$, all the adsorption sites are occupied and stable. Coverages of $\theta > 1$ were not observed as a second layer started to form. Similar to the (001) surface, no reaction between sequential SO molecules was observed on the Pt (011) surface. In the case of the increased surface coverage of $Bridge_{S,O}$, both E_{ads} and sequential E_{ads} decreased as N_{SO} increased. In this case, the adsorption configuration stayed very similar to the single SO adsorption. Higher coverage than $\theta > 1$ was not obtained as a second layer started to form. Again, no reaction between the SO molecules was observed.

Similar to the other surfaces, the (111) surface showed a steady decrease in E_{ads} and sequential E_{ads} as θ increased. At $\theta = 1$, all hcp sites were occupied by SO, but as an additional SO was placed on an *fcc* site, a second SO layer started to form. As with the other surfaces, the subsequent addition of SO molecules did not lead to additional reactions.

Comparing the increased coverage on all three Pt surfaces, it was seen that the highest coverage of SO was achieved on the (001) surface followed by the (011) surface and then the (111) surface.

D. SO_3 adsorption and surface coverage

The literature has shown[19] that five modes of SO_3 adsorption are possible and all were considered in this work, including (i) planar O,O,O, where all four atoms are parallel to the surface, (ii) S,O,O, where only two S–O interact with the surface, (iii) O,O where only two of the O atoms interact, (iv) S,O where one S–O bond interact with the surface and the other two O atoms are directed away from the surface, and (v) where only one O atom interacts with the surface. All five modes were investigated in the various adsorption sites shown in Fig. 1. The most stable structures found for the adsorption of SO_3 onto the Pt surface are shown in Fig. 8, with the adsorption energies, charge transfer, bond distances, and angles of the adsorbed SO_3 with respect to the Pt surfaces listed in Table III.

On the (001) surface, two stable configurations were observed, the most stable being $4F_{S\text{-bound}}$, where the S atom is bound within a 4F hollow, and two O atoms bind to two Pt atoms of the 4F hollow with the third O atom directed toward the vacuum. The second adsorption mode is $Atop_{O,O,O}$, where again the S atom is in the 4F hollow and all three O atoms are bound atop a Pt atom of the 4F hollow. The literature has shown that on the α-Fe_2O_3 (001) surface,[83] an O,O-bridge formed on the surface with a binding energy between −2.27 and −2.46 eV, depending on whether

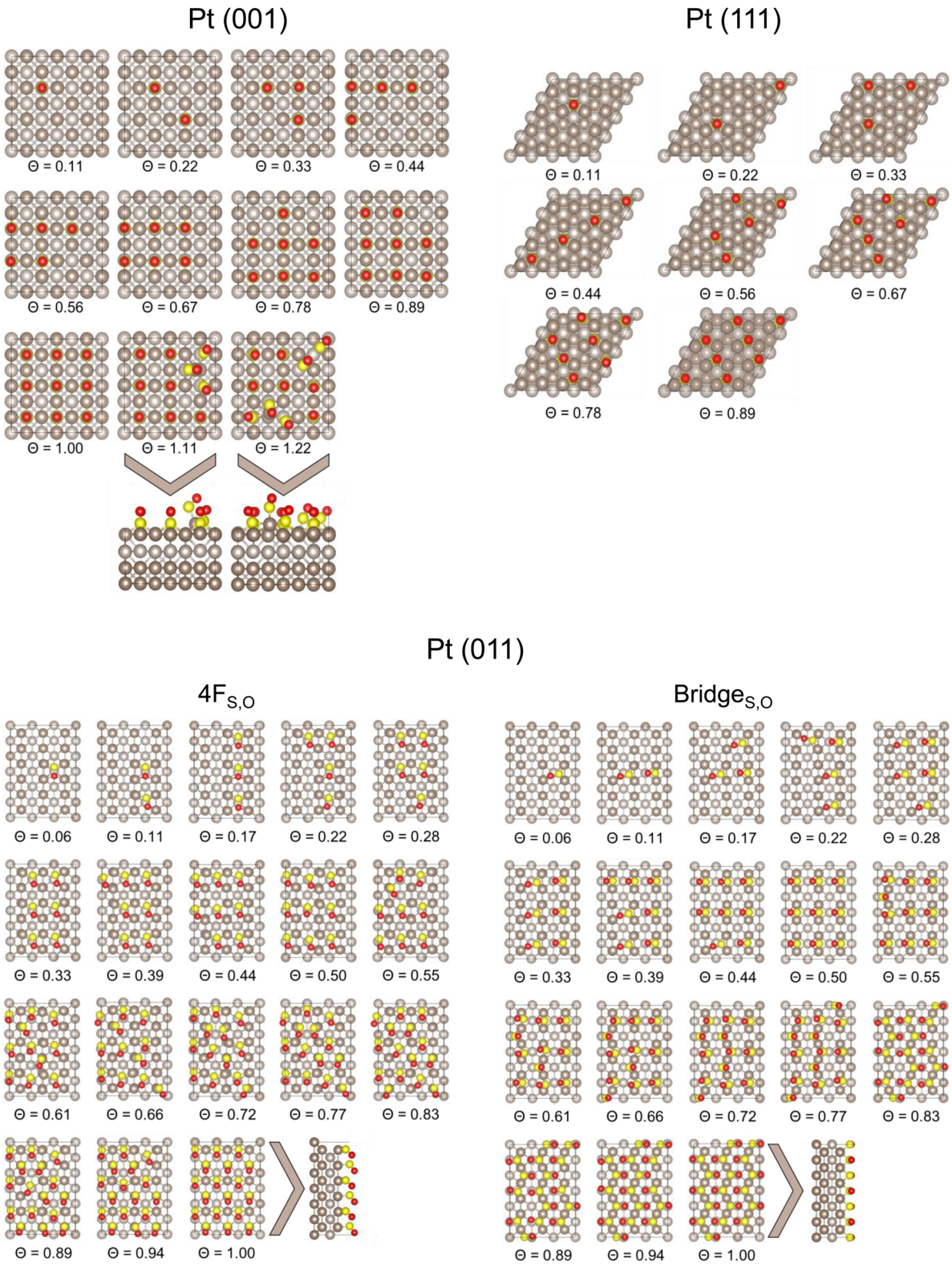

FIG. 6. Increased SO coverage on the Pt (001), (011), and (111) surfaces.

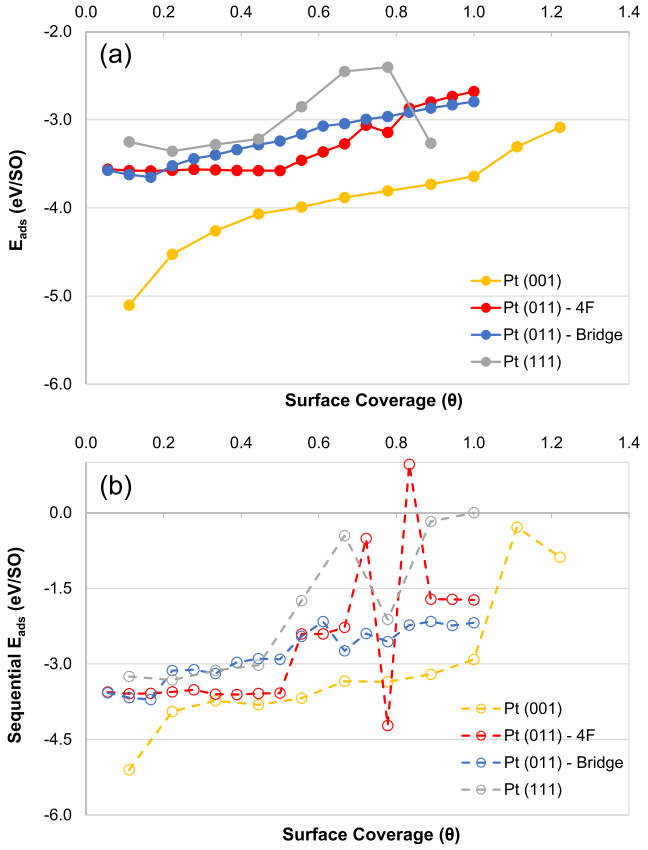

FIG. 7. Average (a) and sequential (b) adsorption energies (E_{ads}) as a function of SO surface coverage (nm^{-2} Pt) on the Pt (001), (011), and (111) surfaces.

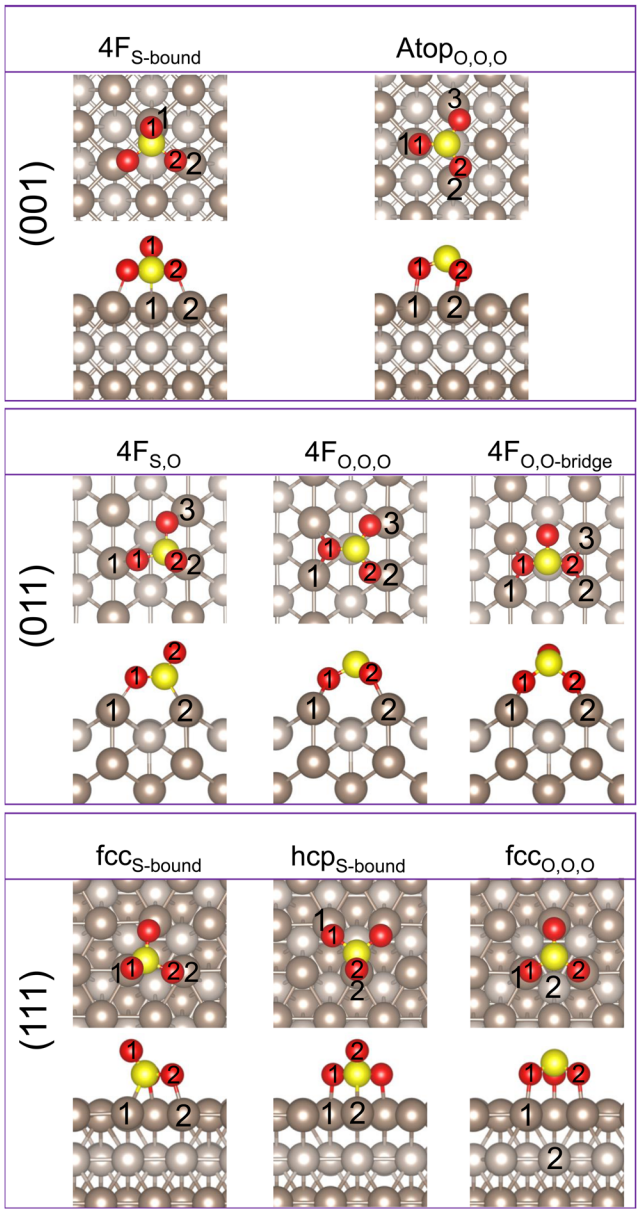

FIG. 8. Stable absorption sites of SO_3 on Pt (001), (011), and (111) surfaces. The atom colors yellow and red denotes sulfur and oxygen atoms, respectively. The numbers (1, 2) indicate the significant Pt or oxygen atoms in the surface (1) or in the second layer (2).

the bridge formed over a Fe–O or Fe–Fe binding site, respectively. Similar to the adsorption of SO on (001), the charge transfer increased as the bond order increased. The free SO_3 molecule showed an average S–O bond length of 1.47 Å and an O–S–O bond angle of 120°, which correlates with the free S–O(1) bond length in the $4F_{S\text{-bound}}$ configuration. In both $4F_{S\text{-bound}}$ and $Atop_{O,O,O}$, the Pt-bound S–O bonds are stretched on average by 0.1 Å. In the $4F_{S\text{-bound}}$ configuration, the planar SO_3 changed to a nearly tetrahedral configuration, causing the O–S–O bond angles to decrease. In addition, in the $Atop_{O,O,O}$ configuration, with the O atoms bound atop the Pt atoms, the S atom is pushed slightly out of plane, decreasing the O–S–O bond angles, which confirms a tetrahedral configuration and indicates that SO_3 is chemisorbed onto the (001) surface.

On the (011) surface, three stable adsorption modes were observed: $4F_{S,O}$, $4F_{O,O,O}$, and $4F_{O,O\text{-bridge}}$. In the first configuration ($4F_{S,O}$), the S atom is bound to one Pt atom on the ridge, one S–O(1) formed a bridge across the (011) ridge and the other S–O(3) formed a bridge on the (011) ridge and oxygen O(2) is directed toward the vacuum. The second stable configuration ($4F_{O,O,O}$), S was over the 4F hollow, with all three O atoms bound to the Pt atoms of the 4F hollow, forming two S–O bridges across the (011) ridge. Similarly, in the third stable configuration, ($4F_{O,O\text{-bridge}}$) S was over the 4F hollow forming two S–O bridges across the (011) ridge, with O(3) directed along the groove of the (011) surface. It has been shown[83] that on the α-Fe_2O_3 (001) surface, Fe–O–Fe binding causes ridges and valleys similar to the (011) surface, and on these Fe–O–Fe binding site, SO_3 forms a stable O,O-bridge across the surface, similar to our $4F_{O,O\text{-bridge}}$ configuration, with a binding energy of −2.27 eV.

The charge transfer between SO_3 and the (011) Pt surface did not follow the same bond order trend as observed for the other adsorptions. Interestingly, more electrons were transferred when

TABLE III. Adsorption energies (E_{ads}), bond distances (d), and angles ($\angle$) of the adsorbed SO_3 on the Pt (001), (011), and (111) surfaces, with the relevant charge transfers (Δq) following adsorption, with $\theta_{(001)/(111)} = 0.11$ and $\theta_{(011)} = 0.06$. The numbers (Pt_1, Pt_2, O_1, O_2, O_3) indicate the significant Pt and O atoms, as shown in Fig. 8.

		(001)		(011)			(111)		
		$4F_S$	$Atop_{O,O,O}$	$4F_{S,O,O}$	$4F_{O,O,O}$	$4F_{O,O\text{-bridge}}$	fcc_S	hcp_S	fcc_O,O,O
	E_{ads} (eV)	−3.38	−2.95	−2.68	−2.18	−1.39	−1.83	−1.79	−1.59
	Δq (e)	−0.60	−0.84	−0.64	−0.86	−0.88	−0.58	−0.57	−0.83
d (Å)	S–Pt_1	2.23	3.12	3.26	3.50	3.55	2.27	2.94	3.16
	S–Pt_2	3.03	3.27	2.23	3.22	3.55	2.95	2.26	3.16
	O_1–Pt_1	3.20	2.10	2.08	2.24	2.18	3.22	2.14	2.11
	O_2–Pt_2	2.10	2.11	3.14	2.10	2.18	2.12	3.23	2.11
	S–O_1	1.44	1.54	1.55	1.62	1.64	1.44	1.54	1.55
	S–O_2	1.55	1.56	1.45	1.53	1.64	1.54	1.44	1.54
∠ (°)	O_1–S–O_2	110.2	106.8	108.0	106.6	105.8	111.1	111.1	107.2
	O_2–S–O_3	107.5	107.6	110.9	108.9	105.2	106.6	107.1	107.2

either just two or all three O atoms were bound to the Pt surface ($4F_{O,O\text{-bridge}}$ and $4F_{O,O,O}$, respectively), compared to when two O atoms and one S atom were bound ($4F_{S,O}$). As observed on the (001) surface, the bound SO_3 configuration changes to a tetrahedral mode, elongating the bound S–O bonds and decreasing the O–S–O bonds, again indicating that SO_3 is chemisorbed onto the (011) surface.

On the (111) surface, three stable adsorption modes were observed, including $fcc_{S\text{-bound}}$, $hcp_{S\text{-bound}}$, and $fcc_{O,O,O}$. The first two are similar, where S is bound over either an *fcc* or *hcp* hollow, with O atoms atop two of the Pt atoms of the hollow adsorption site. In the third adsorption configuration, $fcc_{O,O,O}$, S is again over an *fcc* hollow, with all three O atoms bound atop the surrounding Pt atoms. The $fcc_{S\text{-bound}}$ configuration is similar to our previously predicted SO_2 adsorption on the (111) surface,[47] which had an S,O-bonded geometry on the *fcc* binding site, with one S–O bond in the plane of the surface and the other oxygen directed away from the surface. Lin and co-workers[19] also showed that various adsorption configurations are possible on the (111) surface, with the $fcc_{S\text{-bound}}$ being the most stable with a binding energy of 1.43 eV. They have also shown that the Pt bound S–O bond length is elongated (1.56 Å), while the non-surface bound S–O is similar to the gas phase bond length of S–O (1.46 Å) with a decreased O–S–O bond angle (107°). Similar to the (001) surface, the charge transfer increased as the bond order increased, i.e., $fcc_{S\text{-bound}} > hcp_{S\text{-bound}} > fcc_{O,O,O}$. Chemisorption of SO_3 occurred for all three configurations, and similar to the (001) and (011) surfaces, the Pt bound S–O bond lengths increased and the O–S–O bond angles decreased.

Similar to the adsorption of S, SO, H_2O, and SO_2, the adsorption energy for $N_{SO_3} = 1$ was calculated to be most favorable on the (001) surface followed by the (011) and (111) surfaces.[46–48] The most stable configurations – $(001)_{4F\_S}$, $(011)_{4F\_S,O}$, and $(111)_{fcc\_S}$ – were used to investigate the surface coverage by increasing the number of adsorbed SO_3 molecules ($N_{SO_x}, x = 3$) on each Pt surface, until a monolayer (ML) was obtained. To obtain the lowest energy configurations, shown in Fig. 9, various placements of subsequent SO_3 molecules were considered. To determine if adsorption is still favored as the surface coverage increases, the average adsorption energy [Fig. 10(a)] and the sequential adsorption energy [Fig. 10(b)] as a function of surface coverage were calculated.

As with the adsorption of elemental S and SO on the (001) surface, it can be seen that E_{ads} decreases steadily as the surface coverage increased and is also correlated with the sequential E_{ads} up to $\theta = 0.67$. The initial adsorption configurations up to $\theta = 0.33$ show all SO_3 in the chosen adsorption mode and site of the isolated molecule. At $\theta = 0.44$, the surface becomes more crowded and one of the SO_3 molecules rotates slightly but is still bound in the 4F adsorption site, with two O atoms atop a Pt atom. This slight rotation of the SO_3 molecule adsorption also occurs at higher coverages, possibly causing the smaller adsorption energies. At the highest coverage ($\theta = 0.78$), more distortions can be seen, but no reaction occurred between the SO_3 molecules.

On the Pt (011) surface, E_{ads} again decreases steadily as θ is increased. Furthermore, the sequential E_{ads} also decreases with increased adsorption up to $\theta = 0.39$, but with the addition of another SO_3 ($\theta = 0.44$), the surface becomes more crowded and a slight rotation occurs, causing the sequential E_{ads} to increase. This behavior was repeated with an additional SO_3 ($\theta = 0.50$), causing all SO_3 to have the same orientation as with $N_{SO_3} = 1$, thereby increasing the surface strain and resulting in a smaller sequential E_{ads}. The adsorption of an additional SO_3 at $\theta = 0.55$ caused two SO_3 molecules to react and form SO_4 and SO_2. This secondary reaction caused the sequential E_{ads} to increase. No further SO_3 molecules could be adsorbed as a secondary layer started to form, in addition to secondary reactions occurring.

Similar to the increased coverage of SO_3 on the (001) and (011) surfaces, both E_{ads} and the sequential E_{ads} decreased with increased θ. Coverages of $\theta > 0.44$ were not obtained, as this caused not only secondary layers to form but also the secondary reaction ($2\ SO_3 \rightarrow SO_2 + SO_4$) to occur, as observed on the (011) surface.

When we compare the increased coverages of SO_3 on all three Pt surfaces, we observe that similar to the SO coverages, the highest coverage was achieved on the (001) surface followed by the (011) surface and then the (111) surface. The (011) surface was the most reactive toward secondary reactions between co-adsorbed SO_3 molecules followed by the (111) surface.

E. Thermodynamic influence on adsorption

The HyS cycle is operated at 1 atm (1.103 bar) and 350–400 K. The phase diagrams have therefore been constructed to determine

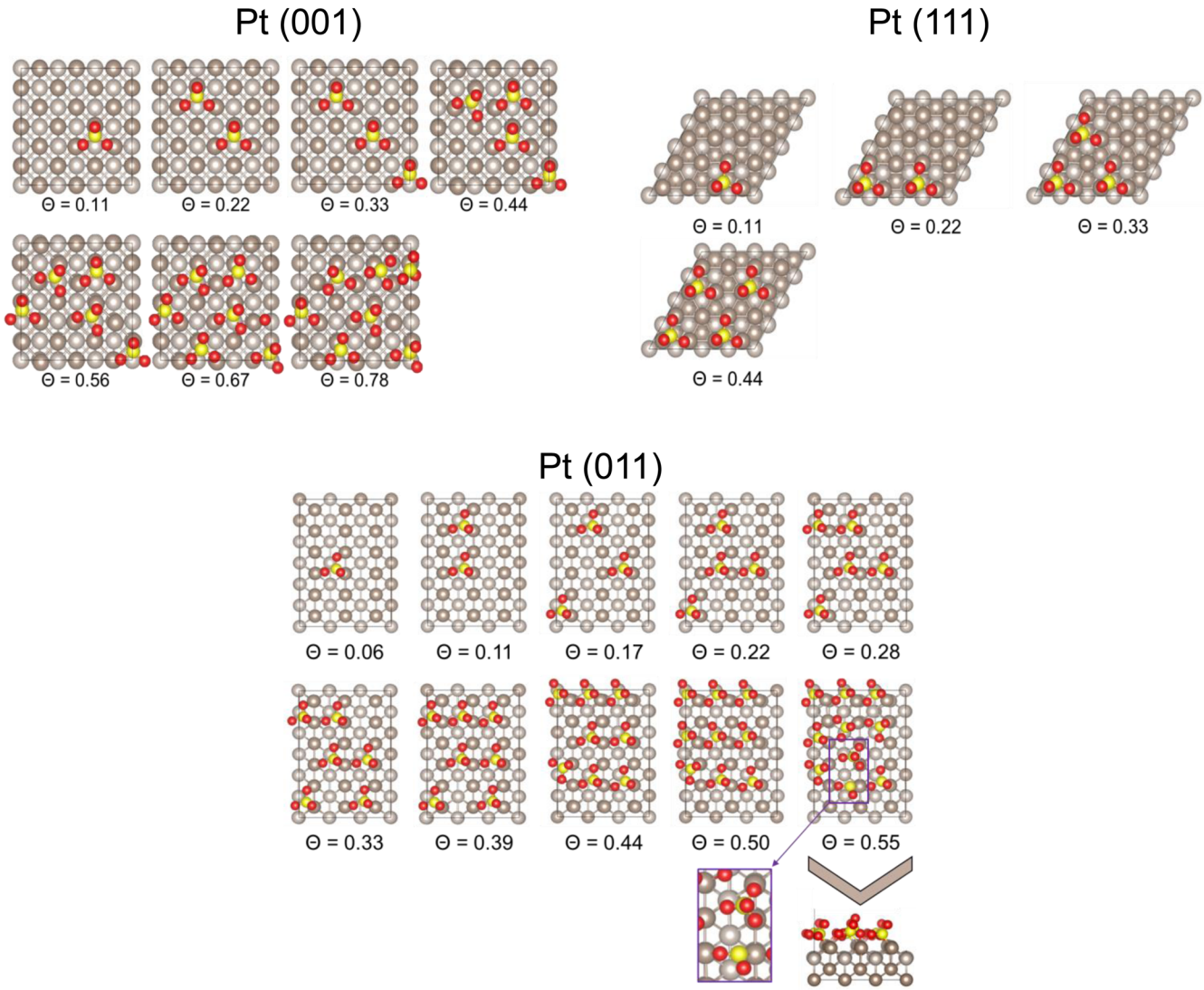

FIG. 9. Increased SO_3 coverage on the Pt (001), (011), and (111) surfaces.

the effect of temperature and pressure on the surface coverage of S, SO, and SO_3. As mentioned, sulfur poisoning may occur on the Pt surface, but we need to establish the effect of temperature and pressure on the surface behavior. Figure 11 shows the phase diagram for S on the Pt (001), (011), and (111) surfaces. Overall, it can be seen that, compared to pressure, temperature has a bigger effect on the S surface coverage.

The adsorption of S onto the surfaces released energies of between 5 and 7 eV (Table I). By adding the thermodynamic terms, it can be seen that the Pt surface is very susceptible to sulfur poisoning under experimental conditions when the surface coverage will be $\theta > 1$. As the temperature increases, subsequent S atoms will react to form S_2 and leave the surface, which is seen at ~700–900 K on the (011) surface, although on the (001) and (111) surfaces, S or S_2 only starts to leave the surface at T > 1300 K. The temperature was only considered up to 2000 K, as Pt starts melting at 2047 K[84] beyond which it can no longer be considered a stable catalyst. The affinity of S adsorption to any Pt surface, even at very high temperatures, is a clear indication that where possible reactions should be designed to prohibit the formation of S as a by-product.

Figure 12 shows the phase diagram for SO on the Pt (001), (011), and (111) surfaces. The thermodynamic data show that for the adsorption of SO on both the (001) and (011) surfaces, coverages of $\theta \geq 1$ can be expected. On the (001) surface, the coverage changes from $\theta = 1.11$ to $\theta = 1.00$ between 250 and 400 K and even up to 1000 K, and the (001) surface will be fully covered with SO. As such, changes in temperature and pressure cannot be utilized to clear the Pt surface of impurities. On the (011) surface, high

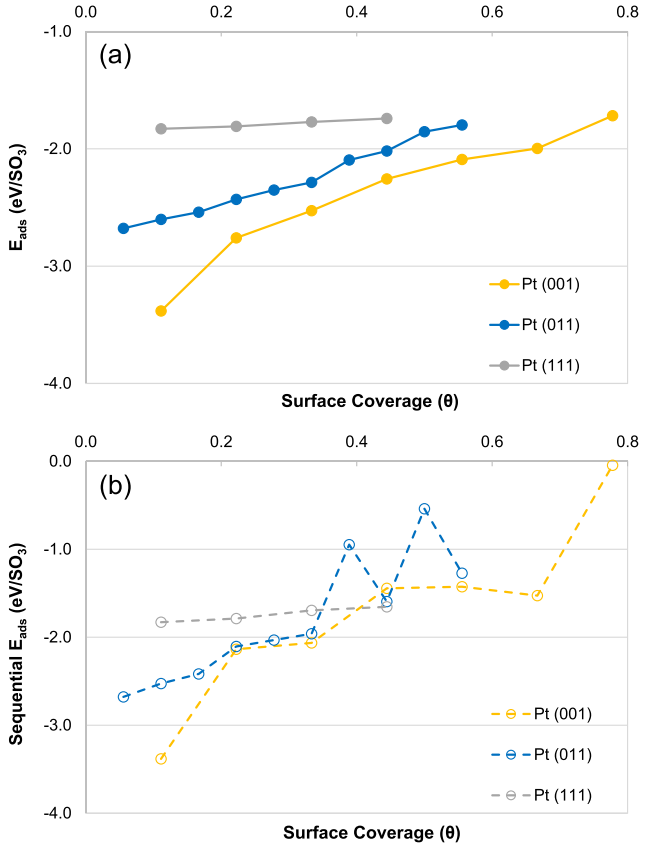

FIG. 10. Average (a) and sequential (b) adsorption energies (E_{ads}) as a function of SO_3 surface coverage (nm^{-2} Pt) on the Pt (001), (011), and (111) surfaces.

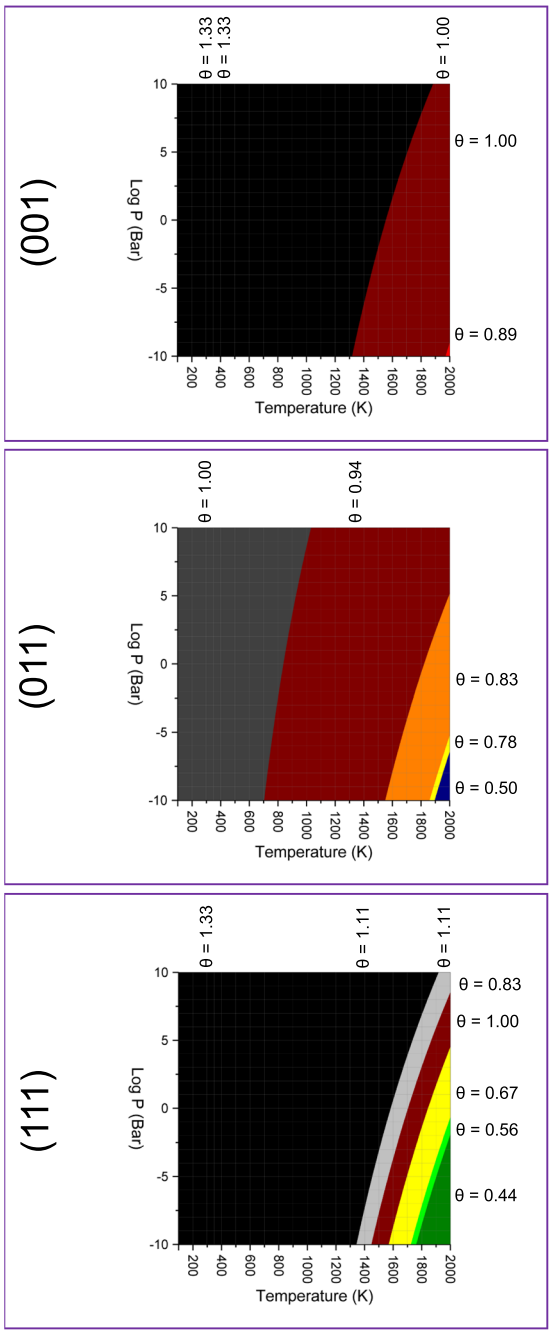

FIG. 11. Surface phase diagrams in terms of pressure and temperature for the surface coverage of S on the Pt (001), (011), and (111) surfaces. The calculated surface coverage (θ) is given for each color.

coverages are sustained up to 350 and 800 K for the SO_{Bridge} and SO_{4F} configurations, respectively. At higher temperatures, some of the SO molecules will leave the surface without taking part in additional reactions, but the surface is never entirely free from SO. Interestingly, on the (111) surface, the SO loading is lower, starting at $\theta = 0.89$ and slowly decreasing to $\theta = 0.44$ at $T \geq 550$ K.

The thermodynamic influence on SO_3 adsorption was also only considered up to 1000 K, as shown in Fig. 13. Similar to the trends with SO, it can be seen in the experimental range (200–400 K), surface coverage is the highest on the (001) surface ($\theta = 0.66$) followed by the (011) ($0.44 < \theta < 0.56$) and (111) ($\theta = 0.44$) surfaces. Here, it can also be seen that temperature has a greater effect on surface coverage, compared to S and SO, possibly due to additional reactions taking place between subsequent SO_3 molecules. Two reactions that may occur include $2\ SO_3 \rightarrow SO$ and SO_4, as was seen on the (011) surface, or $2\ SO_3 \rightarrow 2\ SO_2 + O_2$. The surface can be cleared of SO_3 on both (111) and (011) surfaces at $T \geq 600$ K and $T \geq 800$ K, respectively.

During the investigation of H_2O and SO_2 adsorption on the Pt surfaces,[46–48] temperature played an important role in the surface coverage and that the surface can be cleared of both molecules at elevated temperatures. This is a clear indication that the HyS cycle is temperature sensitive and care should be taken during operation. Elevated temperatures cause first the H_2O molecules will desorb from the surface. This, in turn, could cause an increase in the SO_2 concentration and lead to the formation of more by-products of SO_2, which in turn will impact the efficiency of the HyS cycle.

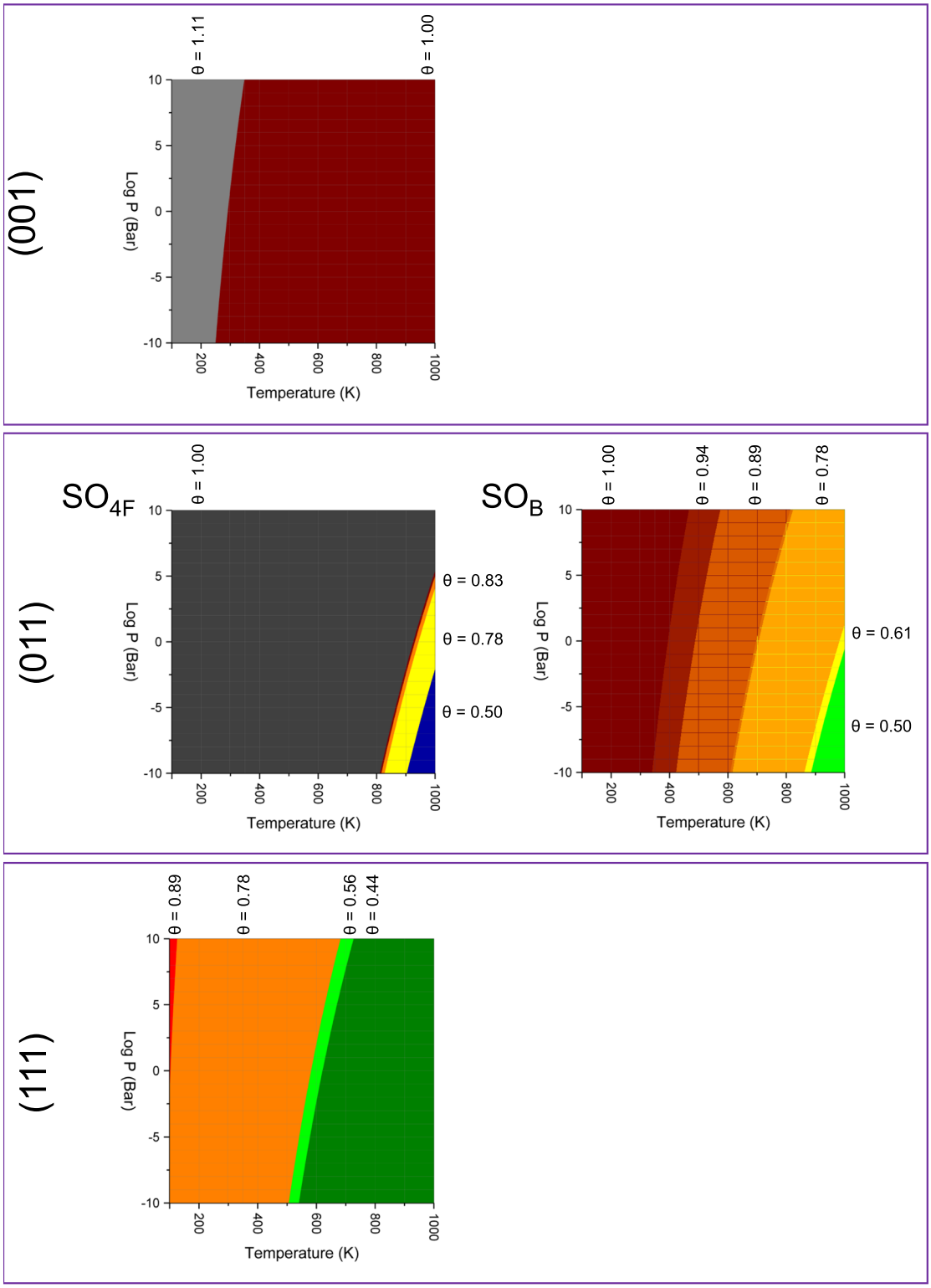

FIG. 12. Surface phase diagrams in terms of pressure and temperature for the surface coverage of SO on the Pt (001), (011), and (111) surfaces. The calculated surface coverage (θ) is given for each color.

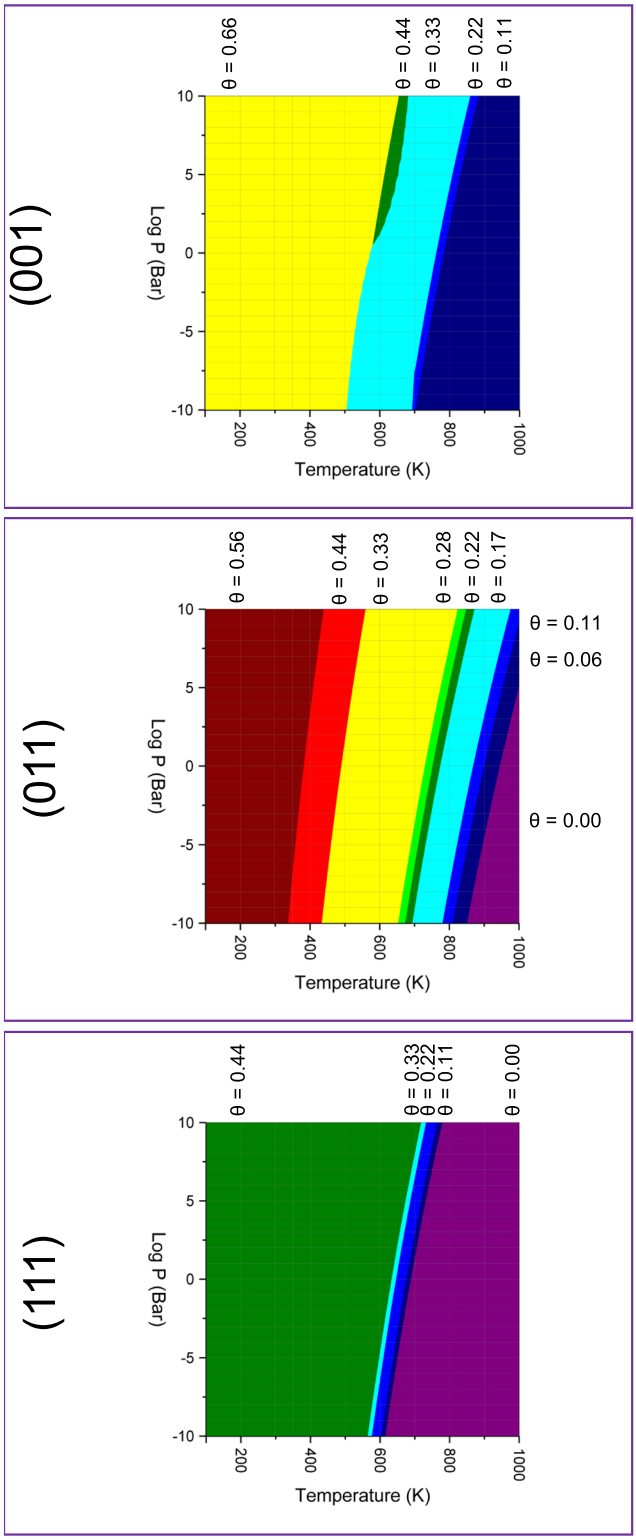

FIG. 13. Surface phase diagrams in terms of pressure and temperature for the surface coverage of SO_3 on the Pt (001), (011), and (111) surfaces. The calculated surface coverage (θ) is given for each color.

IV. CONCLUSIONS

Density functional theory calculations were employed to gain a detailed understanding of the behavior of S, SO, and SO_3 on the Pt (001), (011), and (111) surfaces. Adsorption of all three adsorbates as individual molecules was considered first on all the Pt surfaces. When elemental S was adsorbed, it preferred the 4F hollow site on both the (001) and (011) surfaces (E_{ads_001} = −7.09 eV and E_{ads_011} = −5.47 eV, respectively) and the *fcc* hollow on the (111) surface (E_{ads_111} = −5.47 eV). The adsorption of SO again showed a preference for the 4F hollow on the (001) surface (E_{ads_001} = −5.10 eV), with two possible S,O-adsorptions in the bridge and 4F hollow sites on the (011) surface ($E_{ads\_011\_bridge}$ = −3.56 eV and $E_{ads\_011\_4F}$ = −3.57 eV, respectively) and the *fcc* hollow on the (111) surface (E_{ads_111} = −5.47 eV). Adsorption of SO_3 on the surface was preferred in a S,O,O bound configuration in the 4F (E_{ads_001} = −3.38 eV), 4F (E_{ads_011} = −2.68 eV), and *fcc* (E_{ads_111} = −1.83 eV) hollow adsorption sites on the (001), (011), and (111) surfaces, respectively. Overall, it was found that the higher the bond order, the more the charge transfer occurs from the Pt surface to the adsorbate. In SO_3, in particular, we noted that the molecule configuration changed from planar to tetrahedral, a clear indication of chemisorption and activation of the molecule.

The surface coverage of all three molecules was increased on all the surfaces until a monolayer was obtained. The highest surface coverage for S showed the trend $(001)_S = (111)_S > (011)_S$, and for SO, it was $(001)_{SO} > (011)_{SO} > (111)_{SO}$ and similar for SO_3 $(001)_{SO3} > (011)_{SO3} > (111)_{SO3}$, which indicates that the (001) surface is more susceptible to catalyst poisoning by S species. It was also very evident that both the (001) and (111) surfaces were reactive toward S, leading to the formation of S_2. We found no evidence of secondary reactions of SO on any for the Pt surfaces, but at high coverages of SO_3, we noted the formation of SO_2 and SO_4, especially on the (011) surface.

Thermodynamic effects were also investigated, where we have shown that pressure plays a minimal role in the surface coverage behavior. An increase in the temperature up to 2000 K showed that the Pt surfaces would still be fully covered with S. The SO coverage showed $\theta \geq 1.00$ on both the (001) and (011) surfaces and $\theta = 0.78$ on the (111) surface under the experimental temperature and pressure regime in which the HyS cycle is operated. However, lower coverages of SO_3 were observed and the surface can be cleared at higher temperatures, i.e., $T_{(001)} \geq 1000$ K, $T_{(011)} \geq 800$ K, and $T_{(111)} \geq 600$ K.

ACKNOWLEDGMENTS

We acknowledge the Engineering and Physical Sciences Research Council (EPSRC Grant Nos. EP/K016288/1 and EP/K009567/2) as well as the Economic and Social Research Council (ESRC Grant No. ES/N013867/1) and the National Research Foundation of South Africa for funding under the Newton Programme and for a Post-Doctoral Fellowship (NRF Grant No. 116728). This research was undertaken using resources at North-West University, South Africa, and the Supercomputing Facilities at Cardiff University, UK, operated by ARCCA on behalf of Supercomputing Wales (SCW) projects, which is partly funded by the European Regional Development Fund (ERDF) via Welsh Government. We also acknowledge the use of

facilities at the Centre for High-Performance Computing (CHPC), South Africa.

DATA AVAILABILITY

All data created during this research are openly available from Cardiff University's Research Portal: M. J. Ungerer, C. G. C. E. van Sittert, and N. H. de Leeuw (2021). "Behavior of S, SO, and SO_3 on Pt (001), (011) and (111) surfaces: A DFT Study," Cardiff University's Research Portal, V. 1, Dataset. http://doi.org/10.17035/d.2021.0126222709.

REFERENCES

[1]L. Newman, "Atmospheric oxidation of sulfur dioxide: A review as viewed from power plant and smelter plume studies," Atmos. Environ. **15**, 2231–2239 (1981).
[2]R. E. Huie and P. Neta, "Chemical behavior of sulfur trioxide(1-) (SO_3-) and sulfur pentoxide(1-) (SO_5-) radicals in aqueous solutions," J. Phys. Chem. **88**, 5665–5669 (1984).
[3]"Sulfur," in *Chemistry of the Elements*, 2nd Ed., edited by N. N. Greenwood, A. Earnshaw (Butterworth-Heinemann, 1997), pp. 645–746.
[4]Z. Klimont, S. J. Smith, and J. Cofala, "The last decade of global anthropogenic sulfur dioxide: 2000–2011 emissions," Environ. Res. Lett. **8**, 014003 (2013).
[5]W. Aas, A. Mortier, V. Bowersox, R. Cherian, G. Faluvegi, H. Fagerli, J. Hand, Z. Klimont, C. Galy-Lacaux, C. M. B. Lehmann, C. L. Myhre, G. Myhre, D. Olivié, K. Sato, J. Quaas, P. S. P. Rao, M. Schulz, D. Shindell, R. B. Skeie, A. Stein, T. Takemura, S. Tsyro, R. Vet, and X. Xu, "Global and regional trends of atmospheric sulfur," Sci. Rep. **9**, 953 (2019).
[6]R. H. Michael Gove, Clean Air Strategy Plan, 2019.
[7]Q. Zhong, H. Shen, X. Yun, Y. Chen, Y. Ren, H. Xu, G. Shen, W. Du, J. Meng, W. Li, J. Ma, and S. Tao, "Global sulfur dioxide emissions and the driving forces," Environ. Sci. Technol. **54**, 6508–6517 (2020).
[8]G. L. Smith, J. E. Eyley, X. Han, X. Zhang, J. Li, N. M. Jacques, H. G. W. Godfrey, S. P. Argent, L. J. McCormick McPherson, S. J. Teat, Y. Cheng, M. D. Frogley, G. Cinque, S. J. Day, C. C. Tang, T. L. Easun, S. Rudić, A. J. Ramirez-Cuesta, S. Yang, and M. Schröder, "Reversible coordinative binding and separation of sulfur dioxide in a robust metal–organic framework with open copper sites," Nat. Mater. **18**, 1358–1365 (2019).
[9]S. Díaz-Abad, M. Millán, M. A. Rodrigo, and J. Lobato, "Review of anodic catalysts for SO_2 depolarized electrolysis for 'green hydrogen' production," Catalysts **9**, 63 (2019).
[10]D. R. Uzun, E. Razkazova-Velkova, V. Beschkov, and K. Petrov, "A method for the simultaneous cleansing of H_2S and SO_2," Int. J. Electrochem. **2016**, 1–5.
[11]C.-C. Cormos, "Hydrogen production from fossil fuels with carbon capture and storage based on chemical looping systems," Int. J. Hydrogen Energy **36**, 5960–5971 (2011).
[12]M. Ni, D. Y. C. Leung, M. K. H. Leung, and K. Sumathy, "An overview of hydrogen production from biomass," Fuel Process. Technol. **87**, 461–472 (2006).
[13]C. Acar, I. Dincer, and G. F. Naterer, "Review of photocatalytic water-splitting methods for sustainable hydrogen production," Int. J. Energy Res. **40**, 1449–1473 (2016).
[14]A. Ursúa, L. M. Gandía, and P. Sanchis, "Hydrogen production from water electrolysis: Current status and future trends," Proc. IEEE. **100**, 410–426 (2012).
[15]F. de Bruijn, "The current status of fuel cell technology for mobile and stationary applications," Green Chem. **7**, 132–150 (2005).
[16]L. Baharudin and M. James Watson, "Hydrogen applications and research activities in its production routes through catalytic hydrocarbon conversion," Rev. Chem. Eng. **34**, 43–72 (2017).
[17]L. Schlapbach and A. Züttel, "Hydrogen-storage materials for mobile applications," in *Materials for Sustainable Energy* (Co-published with Macmillan Publishers Ltd, UK, 2010), pp. 265–270.
[18]X. Lin, K. C. Hass, W. F. Schneider, and B. L. Trout, "Chemistry of sulfur oxides on transition metals I: Configurations, energetics, orbital analyses, and surface coverage effects of SO_2 on Pt(111)," J. Phys. Chem. B **106**, 12575–12583 (2002).
[19]X. Lin, W. F. Schneider, and B. L. Trout, "Chemistry of sulfur oxides on transition metals. II. Thermodynamics of sulfur oxides on platinum(111)," J. Phys. Chem. B **108**, 250–264 (2004).
[20]X. Lin, W. F. Schneider, and B. L. Trout, "Chemistry of sulfur oxides on transition metals. III. Oxidation of SO_2 and self-diffusion of O, SO_2, and SO_3 on Pt(111)," J. Phys. Chem. B **108**, 13329–13340 (2004).
[21]J. A. O'Brien, J. T. Hinkley, S. W. Donne, and S.-E. Lindquist, "The electrochemical oxidation of aqueous sulfur dioxide: A critical review of work with respect to the hybrid sulfur cycle," Electrochim. Acta **55**, 573–591 (2010).
[22]M. Polcik, L. Wilde, J. Haase, B. Brena, D. Cocco, G. Comelli, and G. Paolucci, "Adsorption and temperature-dependent decomposition of SO_2 on Cu(100) and Cu(111): A fast and high-resolution core-level spectroscopy study," Phys. Rev. B **53**, 13720–13724 (1996).
[23]M. Polčik, L. Wilde, and J. Haase, "SO_2-induced surface reconstruction of Cu(111): An x-ray-absorption fine-structure study," Phys. Rev. B **57**, 1868–1874 (1998).
[24]M. S. Wilburn and W. S. Epling, "SO_2 adsorption and desorption characteristics of Pd and Pt catalysts: Precious metal crystallite size dependence," Appl. Catal., A **534**, 85–93 (2017).
[25]J. A. Rodriguez, J. M. Ricart, A. Clotet, and F. Illas, "Density functional studies on the adsorption and decomposition of SO_2 on Cu(100)," J. Chem. Phys. **115**, 454–465 (2001).
[26]T. Yokoyama, S. Terada, S. Yagi, A. Imanishi, S. Takenaka, Y. Kitajima, and T. Ohta, "Surface structures and electronic properties of SO_2 adsorbed on Ni(111) and Ni(100) studied by S K-edge X-ray absorption fine structure spectroscopy," Surf. Sci. **324**, 25–34 (1995).
[27]S. Terada, A. Imanishi, T. Yokoyama, S. Takenaka, Y. Kitajima, and T. Ohta, "Surface structure of SO_2 adsorbed on Ni(110) studied by S K-edge X-ray absorption fine structure spectroscopy," Surf. Sci. **336**, 55–62 (1995).
[28]P. Zebisch, M. Weinelt, and H.-P. Steinrück, "Sulphur dioxide adsorption on the Ni(110) surface," Surf. Sci. **295**, 295–305 (1993).
[29]J. Ahner, A. Effendy, K. Vajen, and H.-W. Wassmuth, "Chemisorption and multilayer adsorption of SO_2 on Ag(111) and Ag(110)," Vacuum **41**, 98–101 (1990).
[30]J. L. Solomon, R. J. Madix, W. Wurth, and J. Stohr, "NEXAFS and EELS study of the orientation of sulfur dioxide on silver(110)," J. Phys. Chem. **95**, 3687–3691 (1991).
[31]R. C. Ku and P. Wynblatt, "SO_2 adsorption on Rh(110) and Pt(110) surfaces," Appl. Surf. Sci. **8**, 250–259 (1981).
[32]J. A. Rodriguez, T. Jirsak, and S. Chaturvedi, "Reaction of S_2 and SO_2 with Pd/Rh(111) surfaces: Effects of metal–metal bonding on sulfur poisoning," J. Chem. Phys. **110**, 3138–3147 (1999).
[33]S. Terada, M. Sakano, Y. Kitajima, T. Yokoyama, and T. Ohta, "Adsorption of SO_2 on Pd(100) studied by S K-edge XAFS," J. Phys. IV **7**, C2-703–C2-704 (1997).
[34]M. L. Burke and R. J. Madix, "Hydrogen on Pd(100)-S: The effect of sulfur on precursor mediated adsorption and desorption," Surf. Sci. **237**, 1–19 (1990).
[35]J. M. Saleh, "Interaction of sulphur compounds with palladium," Trans. Faraday Soc. **66**, 242 (1970).
[36]M. L. Burke and R. J. Madix, "SO_2 structure and reactivity on clean and sulfur modified Pd(100)," Surf. Sci. **194**, 223–244 (1988).
[37]S. Astegger and E. Bechtold, "Adsorption of sulfur dioxide and the interaction of coadsorbed oxygen and sulfur on Pt(111)," Surf. Sci. **122**, 491–504 (1982).
[38]U. Köhler and H.-W. Wassmuth, "SO_2 adsorption and desorption kinetics on Pt(111)," Surf. Sci. **126**, 448–454 (1983).
[39]Y.-M. Sun, D. Sloan, D. J. Alberas, M. Kovar, Z.-J. Sun, and J. M. White, "SO_2 adsorption on Pt(111): HREELS, XPS and UPS study," Surf. Sci. **319**, 34–44 (1994).
[40]M. Polčik, L. Wilde, J. Haase, B. Brena, G. Comelli, and G. Paolucci, "High-resolution XPS and NEXAFS study of SO_2 adsorption on Pt(111): Two surface SO_2 species," Surf. Sci. **381**, L568–L572 (1997).
[41]H. R. Colón-Mercado and D. T. Hobbs, "Catalyst evaluation for a sulfur dioxide-depolarized electrolyzer," Electrochem. Commun. **9**, 2649–2653 (2007).
[42]P. W. T. Lu and R. L. Ammon, "An investigation of electrode materials for the anodic oxidation of sulfur dioxide in concentrated sulfuric acid," J. Electrochem. Soc. **127**, 2610 (1980).

[43]A. Appleby and B. Pinchon, "Electrochemical aspects of the $H_2SO_4SO_2$ thermoelectrochemical cycle for hydrogen production," Int. J. Hydrogen Energy **5**, 253–267 (1980).
[44]B. Meyer, "Elemental sulfur," Chem. Rev. **76**, 367–388 (1976).
[45]B. D. Struck, R. Junginger, D. Boltersdorf, and J. Gehrmann, "The anodic oxidation of sulfur dioxide in the sulfuric acid hybrid cycle," Int. J. Hydrogen Energy **5**, 487–497 (1980).
[46]M. J. Ungerer, D. Santos-Carballal, A. Cadi-Essadek, C. G. C. E. van Sittert, and N. H. de Leeuw, "Interaction of H_2O with the platinum Pt (001), (011) and (111) surfaces: A density functional theory study with long-range dispersion corrections," J. Phys. Chem. C **123**(45), 27465 (2019).
[47]M. J. Ungerer, D. Santos-Carballal, A. Cadi-Essadek, C. G. C. E. van Sittert, and N. H. de Leeuw, "Interaction of SO_2 with the platinum (001), (011) and (111) surfaces: A DFT study," Catalysts **10**(5), 558 (2020).
[48]M. J. Ungerer, D. Santos-Carballal, C. G. C. E. van Sittert, and N. H. De Leeuw, "Competitive adsorption of H_2O and SO_2 on catalytic platinum surfaces: A density functional theory study," S. Afr. J. Chem. (published online).
[49]G. Kresse and J. Hafner, "*Ab initio* molecular dynamics for liquid metals," Phys. Rev. B **47**, 558–561 (1993).
[50]G. Kresse and J. Hafner, "*Ab initio* molecular-dynamics simulation of the liquid-metalamorphous- semiconductor transition in germanium," Phys. Rev. B **49**, 14251–14269 (1994).
[51]G. Kresse and J. Furthmüller, "Efficient iterative schemes for *ab initio* total-energy calculations using a plane-wave basis set," Phys. Rev. B **54**, 11169–11186 (1996).
[52]G. Kresse and J. Furthmüller, "Efficiency of ab-initio total energy calculations for metals and semiconductors using a plane-wave basis set," Comput. Mater. Sci. **6**, 15–50 (1996).
[53]P. E. Blöchl, "Projector augmented-wave method," Phys. Rev. B **50**, 17953–17979 (1994).
[54]G. Kresse and D. Joubert, "From ultrasoft pseudopotentials to the projector augmented-wave method," Phys. Rev. B **59**, 1758–1775 (1999).
[55]J. P. Perdew, K. Burke, and M. Ernzerhof, "Generalized gradient approximation made simple," Phys. Rev. Lett. **77**, 3865–3868 (1996).
[56]S. Grimme, S. Ehrlich, and L. Goerigk, "Effect of the damping function in dispersion corrected density functional theory," J. Comput. Chem. **32**, 1456–1465 (2011).
[57]S. Posada-Pérez, D. Santos-Carballal, U. Terranova, A. Roldan, F. Illas, and N. H. de Leeuw, "CO_2 interaction with violarite ($FeNi_2S_4$) surfaces: A dispersion-corrected DFT study," Phys. Chem. Chem. Phys. **20**, 20439–20446 (2018).
[58]S. S. Tafreshi, A. Roldan, N. Y. Dzade, and N. H. de Leeuw, "Adsorption of hydrazine on the perfect and defective copper (111) surface: A dispersion-corrected DFT study," Surf. Sci. **622**, 1–8 (2014).
[59]N. Y. Dzade, A. Roldan, and N. H. de Leeuw, "Activation and dissociation of CO_2 on the (001), (011), and (111) surfaces of mackinawite (FeS): A dispersion-corrected DFT study," J. Chem. Phys. **143**, 094703 (2015).
[60]A. K. Mishra, A. Roldan, and N. H. de Leeuw, "CuO surfaces and CO_2 activation: A dispersion-corrected DFT+U study," J. Phys. Chem. C **120**, 2198–2214 (2016).
[61]S. Grimme, J. Antony, S. Ehrlich, and H. Krieg, "A consistent and accurate *ab initio* parametrization of density functional dispersion correction (DFT-D) for the 94 elements H-Pu," J. Chem. Phys. **132**, 154104 (2010).
[62]M. Methfessel and A. T. Paxton, "High-precision sampling for Brillouin-zone integration in metals," Phys. Rev. B **40**, 3616–3621 (1989).
[63]P. E. Blöchl, O. Jepsen, and O. K. Andersen, "Improved tetrahedron method for Brillouin-zone integrations," Phys. Rev. B **49**, 16223–16233 (1994).
[64]G. Corbel, M. Topić, A. Gibaud, and C. I. Lang, "Selective dry oxidation of the ordered Pt-11.1 at.% v alloy surface evidenced by in situ temperature-controlled X-ray diffraction," J. Alloys Compd. **509**, 6532–6538 (2011).
[65]H. J. Monkhorst and J. D. Pack, "Special points for Brillouin-zon integrations," Phys. Rev. B **13**, 5188–5192 (1976).
[66]J. W. Arblaster, "Crystallographic properties of platinum," Platinum Met. Rev. **41**, 12–21 (1997); available at http://www.technology.matthey.com/article/41/1/12-21/.
[67]J. W. Arblaster, "Crystallographic properties of platinum (errata), platin," Met. Rev. **50**, 118–119 (2006).
[68]G. W. Watson, E. T. Kelsey, N. H. de Leeuw, D. J. Harris, and S. C. Parker, "Atomistic simulation of dislocations, surfaces and interfaces in MgO," J. Chem. Soc. Faraday Trans. **92**, 433 (1996).
[69]G. Henkelman, A. Arnaldsson, and H. Jónsson, "A fast and robust algorithm for Bader decomposition of charge density," Comput. Mater. Sci. **36**, 354–360 (2006).
[70]E. Sanville, S. D. Kenny, R. Smith, and G. Henkelman, "Improved grid-based algorithm for Bader charge allocation," J. Comput. Chem. **28**, 899–908 (2007).
[71]W. Tang, E. Sanville, and G. Henkelman, "A grid-based Bader analysis algorithm without lattice bias," J. Phys.: Condens. Matter. **21**, 084204 (2009).
[72]M. Yu and D. R. Trinkle, "Accurate and efficient algorithm for Bader charge integration," J. Chem. Phys. **134**(6), 064111 (2011).
[73]S. S. Tafreshi, A. Roldan, and N. H. de Leeuw, "Hydrazine network on Cu(111) surface: A density functional theory approach," Surf. Sci. **637-638**, 140–148 (2015).
[74]D. Santos-Carballal, A. Roldan, R. Grau-Crespo, and N. H. de Leeuw, "A DFT study of the structures, stabilities and redox behaviour of the major surfaces of magnetite Fe_3O_4," Phys. Chem. Chem. Phys. **16**, 21082–21097 (2014).
[75]M. Chase, *NIST-JANAF Thermochemical Tables*, 4th ed. (ACS, 1998).
[76]J.-H. Wang and M. Liu, "Computational study of sulfur–nickel interactions: A new S–Ni phase diagram," Electrochem. Commun. **9**, 2212–2217 (2007).
[77]W. R. Tyson and W. A. Miller, "Surface free energies of solid metals: Estimation from liquid surface tension measurements," Surf. Sci. **62**, 267–276 (1977).
[78]Z. Jian-Min, M. Fei, and X. Ke-Wei, "Calculation of the surface energy of fcc metals with modified embedded-atom method," Chin. Phys. **13**, 1082–1090 (2004).
[79]D. R. Alfonso, "Computational studies of experimentally observed structures of sulfur on metal surfaces," J. Phys. Chem. C **115**, 17077–17091 (2011).
[80]C. R. Bernard Rodríguez and J. A. Santana, "Adsorption and diffusion of sulfur on the (111), (100), (110), and (211) surfaces of FCC metals: Density functional theory calculations," J. Chem. Phys. **149**, 204701 (2018).
[81]B. A. Lindquist and T. H. Dunning, "The nature of the SO bond of chlorinated sulfur–oxygen compounds," Theor. Chem. Acc. **133**, 1443 (2014).
[82]R. J. Gillespie and E. A. Robinson, "The sulphur–oxygen bond in sulphuryl and thionyl compounds: Correlation of stretching frequencies and force constants with bond lengths, bond angles, and bond orders," Can. J. Chem. **41**, 2074–2085 (1963).
[83]G. Dai, X. Wang, H. You, Y. Wang, Z. Shan, and H. Tan, "Catalytic function of ferric oxide and effect of water on the formation of sulfur trioxide," J. Environ. Manage. **264**, 110499 (2020).
[84]G. A. Slack, "Platinum as a thermal conductivity standard," J. Appl. Phys. **35**, 339–344 (1964).